A&A 547, A87 (2012)
DOI: 10.1051/0004-6361/201220277

Astronomy & Astrophysics

R-matrix electron-impact excitation data for the B-like iso-electronic sequence⋆

G. Y. Liang[1], N. R. Badnell[2], and G. Zhao[1]

[1] National Astronomical Observatories, CAS, 100012 Beijing, PR China
[2] Department of Physics, University of Strathclyde, Glasgow, G4 0NG, UK
e-mail: gyliang@bao.ac.cn

Received 23 August 2012 / Accepted 25 September 2012

ABSTRACT

We have carried-out parallel intermediate-coupling frame transformation *R*-matrix calculations for electron-impact excitation amongst the 204 close-coupling levels of the $2s^x2p^y$ ($x + y = 3$), $2s^2\{3,4\}l$, $2s2p\{3,4\}l$, and $2p^23l$ configurations for all boron-like ions from C^+ to Kr^{31+}. We have also included the configuration interaction due to the $2p^24l$, $2s3l3l'$ and $2p3s3l$ configurations. A detailed comparison has been made of the target structure and excitation data for four specific ions (viz., Ne^{5+}, Ar^{13+}, Fe^{21+} and Kr^{31+}) that span the sequence, so as to assess the accuracy over the entire sequence. Effective collision strengths (Υs) are presented at temperatures ranging from $2 \times 10^2(z+1)^2$ K to $2 \times 10^6(z+1)^2$ K (where z is the residual charge of the ions, i.e. $Z-5$). Detailed comparisons for the (effective) collision strengths (Υs) Ω are made with the results of previous calculations for the four representative ions. Furthermore, we examine the iso-electronic trends of the effective collision strengths as a function of temperature.

Key words. atomic data – atomic processes – plasmas

1. Introduction

Emission lines of boron-like ions have been recorded in both earlier spacecraft (Malinovsky & Heroux 1973; Huber et al. 1973; Acton et al. 1985) and more recent Hinode/EIS (Brown et al. 2008; Landi & Young 2009; Del Zanna 2012) solar observations. The diagnostic usefulness of B-like $n = 2 \rightarrow n = 2$ transition lines was first noted by Flower & Nussbaumer (1973) for several ions, viz. sodium, silicon, and sulphur. Later, Peng & Pradhan (1995) performed a systematic investigation for line intensity ratios of the boron-like iso-electronic sequence (including C II, N III, O IV, Ne VI, Mg VIII, Al IX, Si X, and S XII), and illustrated some line ratios that are sensitive to electron temperature or electron density. The authors used data from an *R*-matrix calculation by Zhang et al. (1994), which included just the $n = 2$ configurations. However, Keenan et al. (2000, 2002) noticed a slight error by Zhang et al. (1994) when including term coupling coefficients in their *R*-matrix calculation. Keenan et al. (2002) re-calculated the excitation data amongst the fine-structure levels of the $n = 2$ configurations for Si X and S XII. The diagnostic line ratios involving those levels were re-examined by them also and applied to solar observations. Liang & Zhao (2008) furthermore applied the electron density diagnostic line ratio of two 3d−2p transition lines to stellar observations. However, the available excitation data for $n = 2 \rightarrow n = 3$ transitions in the boron-like iso-electronic sequence are mainly from distorted-wave (DW) calculations, which omit the contribution from resonances. In addition to the resonances attached to them, more highly excited states also contribute to lower-lying line ratios via cascades – see for example Del Zanna et al. (2012) and Foster et al. (2012), where R-matrix data were additionally supplemented by DW calculations.

For the astrophysically important Fe^{21+} ion, Badnell et al. (2001) performed a 204-level intermediate-coupling frame transformation (ICFT) *R*-matrix calculation, which included a much larger configuration interaction (CI) expansion. Recently, Liang et al. (2009a, 2011) extended *R*-matrix calculations up to $n = 3$ and 4 for Si^{9+} and S^{11+} ions, respectively. Ludlow et al. (2010) performed Breit-Pauli *R*-matrix calculations for all ions of the argon isonuclear sequence. The boron-like case used a close-coupling expansion comprising the $2s^x2p^y$ ($x + y = 3$), $2s^2\{3,4,5\}l$ configurations. For other ions along this iso-electronic sequence, the distorted-wave calculations performed by Zhang & Sampson (1994a,b) are still the main source of data for various modelling databases, e.g. Chianti v7 (Landi et al. 2012), AtomDB v2[1].

Here, we report on calculations for the electron-impact excitation of the boron-like iso-electronic sequence from C^+ to Kr^{31+} ions that were made using the ICFT *R*-matrix method. This paper is part of our series of works on iso-electronic sequences: Li-like, Liang et al. (2011); F-like, Witthoeft et al. (2007); Ne-like, Liang & Badnell (2010); and Na-like, Liang et al. (2009a,b). This work is part of the UK Atomic Processes for Astrophysical Plasmas (APAP) network[2].

The remainder of this paper is organized as follows. In Sect. 2, we discuss details of the calculational method and pay particular attention to comparing our underlying atomic structure results with those of previous workers. The model for the scattering calculation is outlined in Sect. 3. The excitation results themselves are discussed in Sect. 4.

⋆ These data are made available in the archives of APAP via http://www.apap-network.org, OPEN-ADAS via http://open.adas.ac.uk as well as at the CDS via anonymous ftp to cdsarc.u-strasbg.fr (130.79.128.5) or via http://cdsarc.u-strasbg.fr/viz-bin/qcat?J/A+A/547/A87

[1] http://www.atomdb.org/
[2] http://www.apap-network.org

Table 1. Thomas-Fermi potential scaling factors used in our AUTOSTRUCTURE calculations (see text for details).

Ion	1s	2s	2p	3s	3p	3d	4s	4p	4d	4f
C	1.42633	1.25671	1.19952	1.58317	1.33938	1.25491	1.47430	1.50168	1.41676	1.87478
N	1.42754	1.29142	1.18509	1.55209	1.33194	1.38132	1.53577	1.17635	1.55789	1.95182
O	1.41103	1.24220	1.17671	1.64434	1.34306	1.41337	1.68623	1.29607	1.48413	2.30820
F	1.40597	1.24278	1.17399	1.64015	1.34575	1.43378	1.54779	1.33411	1.48348	2.31452
Ne	1.40173	1.24350	1.17260	1.63435	1.34871	1.44626	1.72622	1.36416	1.52383	3.15127
Na	1.39840	1.24440	1.17205	1.62817	1.35159	1.45478	1.27730	1.54966	1.50999	0.58666
Mg	1.39554	1.24527	1.17189	1.62232	1.35422	1.46091	1.38464	1.31611	1.53481	0.57992
Al	1.39331	1.24606	1.17194	1.61707	1.35664	1.46554	1.44070	1.35498	1.51784	1.12328
Si	1.39126	1.24678	1.17212	1.61234	1.35881	1.46915	1.45299	1.35280	1.53085	1.22926
P	1.38951	1.24743	1.17236	1.60821	1.36083	1.47206	1.46557	1.35802	1.51540	1.33250
Cl	1.38654	1.24854	1.17292	1.60085	1.36417	1.47653	1.47955	1.36821	1.53241	1.44182
Ar	1.38536	1.24902	1.17321	1.59800	1.36562	1.47826	1.48396	1.37121	1.53345	1.47479
K	1.38433	1.24945	1.17349	1.59525	1.36693	1.47974	1.48780	1.37360	1.53422	1.49809
Ca	1.38338	1.24985	1.17377	1.59276	1.36813	1.48103	1.49080	1.37569	1.53488	1.51727
Sc	1.38253	1.25020	1.17403	1.59051	1.36923	1.48216	1.49331	1.37751	1.53545	1.53287
Ti	1.38177	1.25053	1.17428	1.58845	1.37023	1.48318	1.49540	1.37914	1.53595	1.54423
V	1.38108	1.25084	1.17452	1.58660	1.37117	1.48410	1.49729	1.38049	1.53639	1.55359
Cr	1.38045	1.25112	1.17474	1.58487	1.37202	1.48491	1.49872	1.38181	1.53632	1.56402
Mn	1.37987	1.25137	1.17495	1.58327	1.37281	1.48564	1.50016	1.38294	1.53668	1.57186
Fe	1.37933	1.25161	1.17515	1.58174	1.37353	1.48629	1.50142	1.38397	1.53745	1.57746
Co	1.37884	1.25183	1.17534	1.58037	1.37421	1.48690	1.50278	1.38487	1.53772	1.58350
Ni	1.37839	1.25204	1.17552	1.57908	1.37485	1.48746	1.50382	1.38573	1.53800	1.58859
Cu	1.37797	1.25223	1.17570	1.57796	1.37542	1.48796	1.50475	1.38649	1.53824	1.59381
Zn	1.37758	1.25242	1.17586	1.57685	1.37597	1.48843	1.50560	1.38722	1.53845	1.59748
Ga	1.37721	1.25259	1.17601	1.57582	1.37649	1.48887	1.50638	1.38789	1.53866	1.60106
Ge	1.37687	1.25275	1.17616	1.57485	1.37703	1.48933	1.50708	1.38854	1.53885	1.60483
As	1.37655	1.25290	1.17630	1.57395	1.37749	1.48971	1.50774	1.38913	1.53902	1.60791
Se	1.37625	1.25305	1.17643	1.57306	1.37789	1.49002	1.50837	1.38965	1.53918	1.61027
Br	1.37597	1.25318	1.17656	1.57226	1.37829	1.49035	1.50894	1.39015	1.53934	1.61280
Kr	1.37570	1.25330	1.17668	1.57152	1.37868	1.49067	1.50946	1.39063	1.53948	1.61537

2. Sequence calculation

The aim of this work is to perform *R*-matrix calculations employing the ICFT method (see Griffin et al. 1998) for all boron-like ions from C^+ to Kr^{31+}. The close-coupling (CC) expansion we used consists of the $2s^x2p^y$ $(x+y=3)$, $2s^2\{3,4\}l$, $2s2p\{3,4\}l$, and $2p^23l$ (92 LS terms, 204 fine-structure levels) configurations. The additional configuration interaction (CI) from the $2p^24l$, $2s3l3l'$ and $2p3s3l$ (71 LS terms, 160 fine-structure levels) configurations was included for the target structure used in the collision calculation.

2.1. Structure: level energies

The target wavefunctions (1s−4f) were obtained from AUTOSTRUCTURE (AS, Badnell 1986) using the Thomas-Fermi-Dirac-Amaldi model potential. Relativistic effects were included perturbatively from the one-body Breit-Pauli operator (viz. mass-velocity, spin-orbit and Darwin) without valence-electron two-body fine-structure operators. This is consistent with the operators included in the standard Breit-Pauli *R*-matrix suite of codes. The radial scaling parameters, λ_{nl} ($n = 1$−4; $l \in$ s, p, d, and f, were obtained separately for each ion by a three-step optimization procedure. In the first step, the weighted sum of all term energies of the $1s^22s^x2p^y$ $(x+y=3)$ configurations was minimized by varying the λ_{1s}, λ_{2s} and λ_{2p} scaling parameters. Then, the energies of the $1s^22s^23l$ and $1s^22s^24l$ configurations were minimized by varying the λ_{3l} and λ_{4l} scaling parameters, respectively. The resultant scaling parameters are listed in Table 1. For lower charged ions, λ_{4f} is far away from unity. Tests show that it is insensitive to optimization and the atomic structure itself is insensitive to it.

A comparison of level energies is made with the experimentally derived data available from the compilation of NIST v4[3], and with other theoretical results, for four specific ions (Ne^{5+}, Ar^{13+}, Fe^{21+}, and Kr^{31+}) that span the sequence, so as to assess the accuracy of our present structure over the entire iso-electronic sequence – see Tables 2−5. For many excited levels of the $n = 3$ and 4 complexes, the present AS calculation agrees to better than within 1% with the NIST v4[3] recommended values for the four ions. For levels of $n = 2$ configurations, the energy difference is less than 4%. For highly charged ions, this discrepancy becomes smaller. Therefore, we performed a calculation with level energy corrections to the diagonal of the Hamiltonian matrix before diagonalization for the 15 fine-structure levels of the $n = 2$ configurations of almost all ions over the iso-electronic sequence (except for $Z = 29$−35) and iterated to convergence. For those levels missing in the NIST compilation, we adopted the mean value of differences between our level energies and corresponding NIST values of the same configuration. The resulting *e*-vectors and *e*-energies were used to calculate the oscillator strengths and archived energies.

For Ne^{5+}, Mitnik et al. (2001) performed a multi-configuration Hartree-Fock (MCHF) calculation with three pseudo-orbitals ($\overline{5}$s, $\overline{5}$p, and $\overline{5}$d) included, which shows a better agreement with NIST v4 data for the levels of $n = 2$ configurations, see Table 2. For higher excited levels of $n = 3$ and 4 configurations, the two different sets of predictions agree better, to within 1%.

For Ar^{13+}, a GRASP calculation is available, which included the $2s^x2p^y$ $(x+y=3)$, $2s^2\{3,4,5\}l$, $2s2p\{3,4,5\}l$, $2p^2\{3,4,5\}l$ $(l<f)$, and $2s^2\{6,7,8\}$s configurations (Aggarwal et al. 2005).

[3] http://physics.nist.gov/PhysRefData/ASD/index.html

Table 2. Level energies (Ryd) of Ne^{5+} from different calculations, along with the compilation of NIST v4.

ID	Level	AS	NIST	MCHF[a]	ID	Level	AS	NIST	MCHF[a]	ID	Level	AS	NIST	MCHF[a]
1	$2s^22p\ ^2P_{1/2}$	0.0000		0.0000	69	$2s^24d\ ^2D_{5/2}$	9.3126	9.2867	9.3197	137	$2p^23d\ ^2D_{3/2}$	10.3493		10.3924
2	$2s^22p\ ^2P_{3/2}$	0.0118	0.0119	0.0118	70	$2p^23s\ ^4P_{1/2}$	9.3278	9.3111	9.3432	138	$2p^23d\ ^2D_{5/2}$	10.3504		10.3941
3	$2s2p^2\ ^4P_{1/2}$	0.8816	0.9140	0.9078	71	$2p^23s\ ^4P_{3/2}$	9.3320	9.3161	9.3473	139	$2s2p4d\ ^4D_{1/2}$	10.3521	10.3040	10.3360
4	$2s2p^2\ ^4P_{3/2}$	0.8857	0.9180	0.9119	72	$2p^23s\ ^4P_{5/2}$	9.3388	9.3247	9.3540	140	$2s2p4d\ ^4D_{3/2}$	10.3523		10.3362
5	$2s2p^2\ ^4P_{5/2}$	0.8925	0.9239	0.9187	73	$2s2p3d\ ^2D_{3/2}$	9.5013	9.3870	9.5176	141	$2s2p4d\ ^4D_{5/2}$	10.3530		10.3369
6	$2s2p^2\ ^2D_{3/2}$	1.6709	1.6311	1.6799	74	$2s2p3d\ ^2D_{5/2}$	9.5025	9.3883	9.5187	142	$2s2p4d\ ^4D_{7/2}$	10.3563	10.3070	10.3402
7	$2s2p^2\ ^2D_{5/2}$	1.6710	1.6313	1.6800	75	$2p^23s\ ^2P_{1/2}$	9.5542		9.5461	143	$2s2p4d\ ^4P_{5/2}$	10.3650	10.3210	10.3491
8	$2s2p^2\ ^2S_{1/2}$	2.1508	2.1037	2.1959	76	$2s2p3d\ ^2F_{5/2}$	9.5606	9.4480	9.3858	144	$2s2p4d\ ^4P_{3/2}$	10.3677		10.3518
9	$2s2p^2\ ^2P_{1/2}$	2.3465	2.2717	2.3140	77	$2s2p3d\ ^2F_{7/2}$	9.5607	9.4495	9.3859	145	$2s2p4d\ ^4P_{1/2}$	10.3692	10.3230	10.3536
10	$2s2p^2\ ^2P_{3/2}$	2.3545	2.2791	2.3217	78	$2p^23s\ ^2P_{3/2}$	9.5619		9.5536	146	$2s2p4d\ ^2D_{3/2}$	10.3705	10.3120	10.3534
11	$2p^3\ ^4S_{3/2}$	2.9370	2.9307	2.9706	79	$2s2p3d\ ^2P_{1/2}$	9.5991	9.4690	9.6222	147	$2s2p4d\ ^2D_{5/2}$	10.3728	10.3160	10.3556
12	$2p^3\ ^2D_{3/2}$	3.3494	3.2763	3.3347	80	$2s2p3d\ ^2P_{3/2}$	9.6002	9.4699	9.6232	148	$2p^23d\ ^2G_{7/2}$	10.3825		10.4251
13	$2p^3\ ^2D_{5/2}$	3.3497	3.2770	3.3350	81	$2p^23p\ ^2S_{1/2}$	9.6179		9.6137	149	$2p^23d\ ^2G_{9/2}$	10.3846		10.4259
14	$2p^3\ ^2P_{1/2}$	3.7997	3.6998	3.8054	82	$2p^23p\ ^4D_{1/2}$	9.6954	9.6648	9.6905	150	$2p^23p\ ^2P_{1/2}$	10.3882		10.3204
15	$2p^3\ ^2P_{3/2}$	3.8005	3.7002	3.8063	83	$2p^23p\ ^4D_{3/2}$	9.6980	9.6675	9.6930	151	$2p^23p\ ^2P_{3/2}$	10.3929		10.3245
16	$2s^23s\ ^2S_{1/2}$	6.5626	6.5847	6.5970	84	$2p^23p\ ^4D_{5/2}$	9.7022	9.6717	9.6972	152	$2p^23d\ ^2F_{5/2}$	10.3959		10.5083
17	$2s^23p\ ^2P_{1/2}$	7.0079	7.0278	7.0448	85	$2p^23s\ ^2D_{3/2}$	9.7035		9.7313	153	$2p^23d\ ^2F_{7/2}$	10.3965		10.5043
18	$2s^23p\ ^2P_{3/2}$	7.0110	7.0307	7.0473	86	$2p^23s\ ^2D_{5/2}$	9.7038	9.6257	9.7317	154	$2p^23s\ ^2S_{1/2}$	10.4228		10.4056
19	$2s^23d\ ^2D_{3/2}$	7.4272	7.4379	7.4807	87	$2p^23p\ ^4D_{7/2}$	9.7082	9.6775	9.7032	155	$2s2p4f\ ^4G_{5/2}$	10.4354		
20	$2s^23d\ ^2D_{5/2}$	7.4280	7.4386	7.4815	88	$2p^23p\ ^4P_{1/2}$	9.7430	9.7103	9.7367	156	$2s2p4f\ ^4G_{7/2}$	10.4373		
21	$2s2p3s\ ^4P_{1/2}$	7.5851	7.5965	7.6106	89	$2p^23p\ ^4P_{3/2}$	9.7454	9.7114	9.7391	157	$2s2p4f\ ^4G_{9/2}$	10.4403		
22	$2s2p3s\ ^4P_{3/2}$	7.5892	7.6005	7.6146	90	$2p^23p\ ^4P_{5/2}$	9.7496	9.7184	9.7433	158	$2s2p4d\ ^2F_{5/2}$	10.4446	10.3720	10.4208
23	$2s2p3s\ ^4P_{5/2}$	7.5962	7.6079	7.6214	91	$2p^23p\ ^2D_{3/2}$	9.8218	9.7625	9.8091	159	$2s2p4f\ ^4G_{11/2}$	10.4447		
24	$2s2p3s\ ^2P_{1/2}$	7.8114	7.7979	7.8420	92	$2p^23p\ ^2D_{5/2}$	9.8291	9.7712	9.8167	160	$2s2p4d\ ^2F_{7/2}$	10.4508	10.3790	10.4271
25	$2s2p3s\ ^2P_{3/2}$	7.8192	7.8051	7.8495	93	$2p^23p\ ^2P_{1/2}$	9.9038		9.8874	161	$2s2p4f\ ^4F_{3/2}$	10.4553		
26	$2s2p3p\ ^2P_{1/2}$	7.9713	7.9850	7.9990	94	$2p^23p\ ^2P_{3/2}$	9.9045		9.8888	162	$2s2p4f\ ^4F_{5/2}$	10.4561		
27	$2s2p3p\ ^2P_{3/2}$	7.9748	7.9890	8.0025	95	$2p^23p\ ^4S_{3/2}$	9.9734	9.8699	9.9086	163	$2s2p4f\ ^4F_{7/2}$	10.4573		
28	$2s2p3p\ ^4D_{1/2}$	7.9919	7.9980	8.0179	96	$2p^23d\ ^4F_{3/2}$	10.0029		10.0200	164	$2s2p4d\ ^2P_{3/2}$	10.4588		10.4352
29	$2s2p3p\ ^4D_{3/2}$	7.9941	7.9998	8.0201	97	$2p^23d\ ^4F_{5/2}$	10.0050		10.0224	165	$2s2p4f\ ^4F_{9/2}$	10.4592		
30	$2s2p3p\ ^4D_{5/2}$	7.9981	8.0058	8.0240	98	$2p^23d\ ^4F_{7/2}$	10.0082		10.0258	166	$2s2p4d\ ^2P_{1/2}$	10.4628		10.4391
31	$2s2p3p\ ^4D_{7/2}$	8.0041	8.0122	8.0300	99	$2p^23d\ ^4F_{9/2}$	10.0123		10.0303	167	$2s2p4f\ ^2G_{7/2}$	10.4681		
32	$2s2p3p\ ^4S_{3/2}$	8.0788		8.1061	100	$2s2p4s\ ^4P_{1/2}$	10.0376		10.0189	168	$2s2p4f\ ^2G_{9/2}$	10.4726		
33	$2s2p3p\ ^4P_{1/2}$	8.1306	8.1474	8.1800	101	$2s2p4s\ ^4P_{3/2}$	10.0414		10.0229	169	$2s2p4f\ ^4D_{7/2}$	10.4819		
34	$2s2p3p\ ^4P_{3/2}$	8.1336	8.1504	8.1827	102	$2s2p4s\ ^4P_{5/2}$	10.0479		10.0296	170	$2s2p4f\ ^4D_{5/2}$	10.4844		
35	$2s2p3p\ ^4P_{5/2}$	8.1378	8.1543	8.1866	103	$2p^23d\ ^4D_{1/2}$	10.0726		10.0744	171	$2s2p4f\ ^4D_{3/2}$	10.4860		
36	$2s2p3p\ ^2D_{3/2}$	8.2059	8.2023	8.2418	104	$2p^23d\ ^4D_{3/2}$	10.0735		10.0758	172	$2s2p4f\ ^4D_{1/2}$	10.4869		
37	$2s2p3p\ ^2D_{5/2}$	8.2131	8.2110	8.2490	105	$2p^23d\ ^4D_{5/2}$	10.0751		10.0781	173	$2p^23d\ ^2D_{3/2}$	10.5011	10.4050	10.5033
38	$2s2p3p\ ^2S_{1/2}$	8.3490	8.3368	8.3828	106	$2p^23d\ ^4D_{7/2}$	10.0770		10.0807	174	$2p^23d\ ^2D_{5/2}$	10.5012		10.5035
39	$2s2p3d\ ^4F_{3/2}$	8.3692	8.3540	8.3809	107	$2p^23p\ ^2F_{5/2}$	10.0918	9.9862	10.0984	175	$2s2p4f\ ^2D_{5/2}$	10.5790		
40	$2s2p3d\ ^4F_{5/2}$	8.3715	8.3566	8.3834	108	$2p^23p\ ^2F_{7/2}$	10.0942	9.9890	10.1004	176	$2s2p4f\ ^2D_{3/2}$	10.5791	10.4590	
41	$2s2p3d\ ^4F_{7/2}$	8.3749	8.3621	8.3868	109	$2p^23d\ ^2P_{3/2}$	10.1044		10.0845	177	$2s2p4f\ ^2F_{7/2}$	10.5951		
42	$2s2p3d\ ^4F_{9/2}$	8.3793	8.3669	8.3914	110	$2p^23d\ ^2P_{1/2}$	10.1100		10.0900	178	$2s2p4f\ ^2F_{5/2}$	10.5957	10.4570	
43	$2s2p3d\ ^4D_{1/2}$	8.4651	8.4420	8.4739	111	$2p^23d\ ^2F_{5/2}$	10.1113	10.0530	10.1527	179	$2p^23d\ ^2P_{1/2}$	10.6165		10.6208
44	$2s2p3d\ ^4D_{3/2}$	8.4658	8.4420	8.4746	112	$2s2p4s\ ^2P_{1/2}$	10.1164		10.0871	180	$2p^23d\ ^2P_{3/2}$	10.6193		10.6233
45	$2s2p3d\ ^4D_{5/2}$	8.4671	8.4430	8.4759	113	$2p^23d\ ^2F_{7/2}$	10.1184	10.0614	10.1608	181	$2p^23d\ ^2S_{1/2}$	10.6838		10.6831
46	$2s2p3d\ ^4D_{7/2}$	8.4694	8.4457	8.4782	114	$2s2p4s\ ^2P_{3/2}$	10.1222		10.0931	182	$2p^23p\ ^2P_{1/2}$	10.8101		10.8195
47	$2s2p3d\ ^2D_{3/2}$	8.4892	8.4568	8.5025	115	$2p^23d\ ^4P_{5/2}$	10.1866	10.1320	10.1628	183	$2p^23p\ ^2P_{3/2}$	10.8112		10.8208

Notes. [a] MCHF calculation from the work of Mitnik et al. (2001).

Table 3. Level energies (Ryd) of Ar^{13+} from different calculations, along with the compilation of NIST v4.

ID	Level	AS	NIST	Grasp[a]	ID	Level	AS	NIST	Grasp[a]	ID	Level	AS	NIST	Grasp[a]
1	$2s^22p\ ^2P_{1/2}$	0	0.0000	0.0000	69	$2p^23s\ ^2P_{1/2}$	37.5209		37.5292	137	$2s2p4s\ ^2P_{3/2}$	44.7689		44.6686
2	$2s^22p\ ^2P_{3/2}$	0.2042	0.2065	0.2055	70	$2s2p3d\ ^2D_{5/2}$	37.5231		37.4763	138	$2s2p4p\ ^4D_{1/2}$	44.8047		44.6978
3	$2s2p^2\ ^4P_{1/2}$	2.0487	2.0986	2.0602	71	$2p^23s\ ^2P_{3/2}$	37.6311		37.6372	139	$2s2p4p\ ^4D_{3/2}$	44.8466		44.7408
4	$2s2p^2\ ^4P_{3/2}$	2.1269	2.1775	2.1379	72	$2s2p3d\ ^2P_{1/2}$	37.6810		37.6364	140	$2s2p4p\ ^2P_{3/2}$	44.9044		44.7968
5	$2s2p^2\ ^4P_{5/2}$	2.2390	2.2820	2.2422	73	$2s2p3d\ ^2P_{3/2}$	37.7054		37.6586	141	$2s2p4p\ ^4D_{5/2}$	44.9078		44.8038
6	$2s2p^2\ ^2D_{3/2}$	3.7691	3.7385	3.7798	74	$2p^23p\ ^2S_{1/2}$	37.7337		37.6969	142	$2s2p4p\ ^2P_{1/2}$	44.9231		44.8158
7	$2s2p^2\ ^2D_{5/2}$	3.7809	3.7471	3.7879	75	$2p^23p\ ^4D_{1/2}$	37.8113		37.7775	143	$2s2p4p\ ^4P_{1/2}$	44.9728		44.8683
8	$2s2p^2\ ^2S_{1/2}$	4.7322	4.6876	4.7584	76	$2p^23p\ ^4D_{3/2}$	37.8531		37.8183	144	$2s2p4p\ ^4S_{3/2}$	44.9989		44.8939
9	$2s2p^2\ ^2P_{1/2}$	5.0260	4.9686	5.0489	77	$2p^23s\ ^2D_{5/2}$	37.8903		37.9098	145	$2s2p4p\ ^4D_{7/2}$	45.0193		44.9248
10	$2s2p^2\ ^2P_{3/2}$	5.1212	5.0546	5.1382	78	$2p^23s\ ^2D_{3/2}$	37.9052		37.9252	146	$2s2p4p\ ^4P_{3/2}$	45.0777		44.9822
11	$2p^3\ ^4S_{3/2}$	6.5409	6.5513	6.5551	79	$2p^23p\ ^4D_{5/2}$	37.9303		37.8961	147	$2s2p4p\ ^4P_{5/2}$	45.0901		44.9931
12	$2p^3\ ^2D_{3/2}$	7.4504	7.3848	7.4625	80	$2p^23p\ ^4P_{1/2}$	38.0183		37.9839	148	$2s2p4p\ ^2D_{3/2}$	45.1040		45.0026
13	$2p^3\ ^2D_{5/2}$	7.4754	7.4082	7.4785	81	$2p^23p\ ^4P_{3/2}$	38.0275		37.9903	149	$2s2p4d\ ^4F_{3/2}$	45.1507		45.0389
14	$2p^3\ ^2P_{1/2}$	8.3694	8.2815	8.3882	82	$2p^23p\ ^4D_{7/2}$	38.0326		37.9964	150	$2s2p4d\ ^4F_{5/2}$	45.1812		45.0696
15	$2p^3\ ^2P_{3/2}$	8.4117	8.3204	8.4259	83	$2p^23p\ ^4P_{5/2}$	38.0846		38.0481	151	$2s2p4p\ ^2D_{5/2}$	45.1930		45.0939
16	$2s^23s\ ^2S_{1/2}$	31.1413		31.0761	84	$2p^23p\ ^2D_{3/2}$	38.1537		38.1159	152	$2s2p4d\ ^4F_{7/2}$	45.2332		45.1230
17	$2s^23p\ ^2P_{1/2}$	32.1745	32.2032	32.1137	85	$2p^23p\ ^2D_{5/2}$	38.2960		38.2631	153	$2s2p4d\ ^4P_{5/2}$	45.2639		45.1525
18	$2s^23p\ ^2P_{3/2}$	32.2315	32.2118	32.1704	86	$2p^23p\ ^2P_{3/2}$	38.4492		38.4071	154	$2s2p4d\ ^4D_{3/2}$	45.2810		45.1708
19	$2s^23d\ ^2D_{3/2}$	33.2077	33.174	33.1377	87	$2p^23p\ ^2P_{1/2}$	38.4796		38.4437	155	$2s2p4d\ ^4D_{1/2}$	45.2887		45.1793
20	$2s^23d\ ^2D_{5/2}$	33.2250	33.186	33.1534	88	$2p^23p\ ^4S_{3/2}$	38.4996		38.4344	156	$2s2p4p\ ^2S_{1/2}$	45.2917		45.1874
21	$2s2p3s\ ^4P_{1/2}$	33.2554		33.2260	89	$2p^23d\ ^4F_{3/2}$	38.6220		38.5675	157	$2s2p4d\ ^4F_{9/2}$	45.3367		45.2354
22	$2s2p3s\ ^4P_{3/2}$	33.3203		33.2905	90	$2p^23d\ ^4F_{5/2}$	38.6628		38.6081	158	$2s2p4d\ ^2D_{3/2}$	45.3381		45.2297
23	$2s2p3s\ ^4P_{5/2}$	33.4459		33.4203	91	$2p^23d\ ^4F_{7/2}$	38.7231		38.6686	159	$2s2p4d\ ^2D_{5/2}$	45.3749		45.2673
24	$2s2p3s\ ^2P_{1/2}$	33.7854	33.770	33.7704	92	$2p^23p\ ^2F_{5/2}$	38.7749		38.7472	160	$2s2p4d\ ^4D_{7/2}$	45.3949		45.2936
25	$2s2p3s\ ^2P_{3/2}$	33.9241	33.907	33.9114	93	$2p^23d\ ^4F_{9/2}$	38.8036		38.7474	161	$2s2p4f\ ^4G_{5/2}$	45.4064		45.2902
26	$2s2p3p\ ^4D_{1/2}$	34.1806		34.1368	94	$2p^23p\ ^2F_{7/2}$	38.8171		38.7860	162	$2s2p4f\ ^4F_{7/2}$	45.4115		45.2953
27	$2s2p3p\ ^4D_{3/2}$	34.2389		34.1935	95	$2p^23d\ ^2P_{3/2}$	38.8390		38.8772	163	$2s2p4d\ ^4D_{5/2}$	45.4200		45.3191
28	$2s2p3p\ ^2P_{1/2}$	34.3050		34.2670	96	$2p^23d\ ^4D_{1/2}$	38.8496		38.8025	164	$2s2p4d\ ^4P_{3/2}$	45.4308		45.3315
29	$2s2p3p\ ^2P_{3/2}$	34.3263		34.2885	97	$2p^23d\ ^4D_{5/2}$	38.8824		38.8298	165	$2s2p4d\ ^4P_{1/2}$	45.4367		45.3386
30	$2s2p3p\ ^4D_{5/2}$	34.3357		34.2915	98	$2p^23d\ ^4D_{7/2}$	38.9205		38.8681	166	$2s2p4f\ ^4F_{3/2}$	45.4553		45.3422
31	$2s2p3p\ ^4D_{7/2}$	34.4471		34.4066	99	$2p^23d\ ^4D_{3/2}$	38.9276		38.7878	167	$2s2p4f\ ^4F_{9/2}$	45.4629		45.3485
32	$2s2p3p\ ^4S_{3/2}$	34.5295		34.4901	100	$2p^23d\ ^2F_{5/2}$	38.9692		38.9235	168	$2s2p4f\ ^4F_{5/2}$	45.4654		45.3509
33	$2s2p3p\ ^4P_{1/2}$	34.5983		34.6001	101	$2p^23d\ ^2P_{1/2}$	39.0329		38.9860	169	$2s2p4f\ ^2F_{7/2}$	45.4713		45.3560
34	$2s2p3p\ ^4P_{3/2}$	34.6747		34.6734	102	$2p^23d\ ^2F_{7/2}$	39.1120		39.0710	170	$2s2p4f\ ^2F_{5/2}$	45.4995		45.3846
35	$2s2p3p\ ^4P_{5/2}$	34.7237		34.7226	103	$2p^23p\ ^2D_{3/2}$	39.1312		39.0691	171	$2s2p4f\ ^2G_{7/2}$	45.5006		45.3863
36	$2s2p3p\ ^2D_{3/2}$	34.7765	34.891	34.7586	104	$2p^23p\ ^2D_{5/2}$	39.1428		39.0760	172	$2s2p4d\ ^2F_{5/2}$	45.5250		45.4170
37	$2s2p3p\ ^2D_{5/2}$	34.9012		34.8907	105	$2p^23d\ ^4P_{5/2}$	39.1655		39.1089	173	$2s2p4d\ ^2P_{3/2}$	45.5864		45.4808
38	$2s2p3d\ ^4F_{3/2}$	35.0879		35.0216	106	$2p^23d\ ^4P_{3/2}$	39.2075		39.1535	174	$2s2p4f\ ^4G_{9/2}$	45.5976		45.4937
39	$2s2p3d\ ^4F_{5/2}$	35.1274		35.0603	107	$2p^23d\ ^4P_{1/2}$	39.2208		39.1733	175	$2s2p4f\ ^4G_{7/2}$	45.6032		45.4994
40	$2s2p3p\ ^2S_{1/2}$	35.1719		35.1594	108	$2p^23s\ ^2S_{1/2}$	39.2456		39.2393	176	$2s2p4d\ ^2F_{7/2}$	45.6140		45.5083
41	$2s2p3d\ ^4F_{7/2}$	35.1869		35.1203	109	$2p^23p\ ^2P_{1/2}$	39.3396		39.2804	177	$2s2p4f\ ^4G_{11/2}$	45.6166		45.5121
42	$2s2p3d\ ^4F_{9/2}$	35.2756		35.2137	110	$2p^23p\ ^2P_{3/2}$	39.4393		39.3833	178	$2s2p4f\ ^4D_{5/2}$	45.6192		45.5151
43	$2s2p3d\ ^4D_{5/2}$	35.3938		35.3228	111	$2p^23d\ ^2G_{7/2}$	39.5719		39.5341	179	$2s2p4f\ ^4D_{7/2}$	45.6223		45.5180
44	$2s2p3d\ ^4D_{3/2}$	35.4004		35.3304	112	$2p^23d\ ^2G_{9/2}$	39.5943		39.5529	180	$2s2p4f\ ^4D_{3/2}$	45.6383		45.5346
45	$2s2p3d\ ^4D_{1/2}$	35.4017		35.3326	113	$2p^23d\ ^2D_{5/2}$	39.6243		39.5672	181	$2s2p4d\ ^2P_{1/2}$	45.6392		45.5358
46	$2s2p3s\ ^2P_{1/2}$	35.4221		35.4359	114	$2p^23d\ ^2D_{3/2}$	39.6340		39.5765	182	$2s2p4f\ ^2G_{9/2}$	45.6448		45.5417
47	$2s2p3s\ ^2P_{3/2}$	35.4253		35.4455	115	$2p^23d\ ^2D_{3/2}$	39.8090		39.7694	183	$2s2p4f\ ^4D_{1/2}$	45.6497		45.5466

Notes. [(a)] GRASP calculation from the work of Aggarwal et al. (2005).

Table 4. Level energies (Ryd) of Fe^{21+} from different calculations, along with the compilation of NIST v4.

ID	Level	AS	NIST	MCDF[a]	ID	Level	AS	NIST	MCDF[a]	ID	Level	AS	NIST	MCDF[a]
1	$2s^22p\ ^2P_{1/2}$	0	0	0.0000	69	$2p^23p\ ^4D_{1/2}$	84.5624		84.4349	137	$2s2p4p\ ^4D_{3/2}$	104.4113		104.1392
2	$2s^22p\ ^2P_{3/2}$	1.0603	1.0777	1.0749	70	$2s2p3d\ ^2D_{3/2}$	84.5817	83.2350	84.4171	138	$2s2p4p\ ^4S_{3/2}$	104.5214		104.2467
3	$2s2p^2\ ^4P_{1/2}$	3.6179	3.6865	3.6715	71	$2s2p3d\ ^2D_{5/2}$	84.7042	84.4930	84.5368	139	$2s2p4s\ ^4P_{5/2}$	104.6367		104.4038
4	$2s2p^2\ ^4P_{3/2}$	4.1160	4.1936	4.1739	72	$2p^23s\ ^2P_{3/2}$	84.7790		84.7350	140	$2s2p4p\ ^4P_{1/2}$	104.6684		104.4069
5	$2s2p^2\ ^4P_{5/2}$	4.6268	4.6772	4.6592	73	$2s2p3d\ ^2P_{1/2}$	84.8978		84.7374	141	$2s2p4p\ ^4D_{5/2}$	104.6745		104.4069
6	$2s2p^2\ ^2D_{3/2}$	6.7138	6.7097	6.7573	74	$2s2p3d\ ^2P_{3/2}$	84.9134	83.5450	84.7548	142	$2s2p4p\ ^2P_{1/2}$	104.7030	104.4770	104.4356
7	$2s2p^2\ ^2D_{5/2}$	6.9224	6.9184	6.9597	75	$2p^23p\ ^4D_{3/2}$	85.0519		84.9179	143	$2s2p4p\ ^2D_{3/2}$	104.7944	104.5590	104.5288
8	$2s2p^2\ ^2P_{1/2}$	7.7937	7.7790	7.8543	76	$2p^23p\ ^2S_{1/2}$	85.0774		84.9893	144	$2s2p4s\ ^2P_{3/2}$	104.8556		104.6279
9	$2s2p^2\ ^2S_{1/2}$	8.9126	8.9154	8.9875	77	$2p^23p\ ^4P_{3/2}$	85.4102		85.2964	145	$2s2p4d\ ^4F_{3/2}$	104.8838		104.5975
10	$2s2p^2\ ^2P_{3/2}$	9.0649	9.0427	9.1189	78	$2p^23p\ ^4D_{5/2}$	85.4840		85.3815	146	$2s2p4d\ ^4F_{5/2}$	104.9892	104.7230	104.7029
11	$2p^3\ ^4S_{3/2}$	11.3938	11.4428	11.4835	79	$2p^23s\ ^2D_{5/2}$	85.5691		85.5353	147	$2s2p4d\ ^4P_{5/2}$	105.1786		104.8957
12	$2p^3\ ^2D_{3/2}$	12.7219	12.7223	12.8095	80	$2p^23p\ ^4P_{1/2}$	85.6311		85.5281	148	$2s2p4d\ ^4F_{7/2}$	105.2299		104.9450
13	$2p^3\ ^2D_{5/2}$	13.0256	12.9999	13.0827	81	$2p^23p\ ^4P_{5/2}$	85.6854		85.5701	149	$2s2p4d\ ^4D_{3/2}$	105.2456	105.0330	104.9663
14	$2p^3\ ^2P_{1/2}$	14.3269	14.3035	14.4203	82	$2p^23s\ ^2D_{3/2}$	85.7357		85.7201	150	$2s2p4d\ ^4D_{1/2}$	105.2721		104.9952
15	$2p^3\ ^2P_{3/2}$	14.8546	14.8329	14.9376	83	$2p^23p\ ^2D_{3/2}$	85.8232		85.7121	151	$2s2p4f\ ^4G_{5/2}$	105.2994		104.9986
16	$2s^23s\ ^2S_{1/2}$	74.0596		73.9173	84	$2p^23p\ ^4D_{7/2}$	85.9122		85.7926	152	$2s2p4f\ ^4D_{7/2}$	105.3225		105.0197
17	$2s^23p\ ^2P_{1/2}$	75.7060		75.5693	85	$2p^23d\ ^4F_{3/2}$	86.2029		86.0427	153	$2s2p4p\ ^4P_{3/2}$	105.3669		105.1482
18	$2s^23p\ ^2P_{3/2}$	76.0015		75.8716	86	$2p^23p\ ^4S_{3/2}$	86.3421		86.2111	154	$2s2p4p\ ^4D_{7/2}$	105.3806		105.1590
19	$2s2p3s\ ^4P_{1/2}$	77.3238		77.2006	87	$2p^23p\ ^2D_{5/2}$	86.4269		86.3172	155	$2s2p4d\ ^2D_{3/2}$	105.3863		105.1110
20	$2s^23d\ ^2D_{3/2}$	77.5321	77.4390	77.3765	88	$2p^23d\ ^4F_{5/2}$	86.4297		86.2656	156	$2s2p4p\ ^4P_{5/2}$	105.4009		105.1821
21	$2s2p3s\ ^4P_{3/2}$	77.6028		77.4768	89	$2p^23p\ ^2P_{3/2}$	86.4414		86.3180	157	$2s2p4d\ ^2F_{5/2}$	105.4523	105.3240	105.1722
22	$2s^23d\ ^2D_{5/2}$	77.6273	77.5210	77.4663	90	$2p^23p\ ^2P_{1/2}$	86.7021		86.6090	158	$2s2p4p\ ^2P_{3/2}$	105.4671		105.2461
23	$2s2p3s\ ^2P_{1/2}$	78.2248		78.1605	91	$2p^23d\ ^4F_{7/2}$	86.8421		86.7002	159	$2s2p4f\ ^4F_{3/2}$	105.5584		105.2649
24	$2s2p3s\ ^4P_{5/2}$	78.3315		78.2274	92	$2p^23d\ ^2P_{3/2}$	86.8509		86.7206	160	$2s2p4f\ ^4G_{7/2}$	105.5734		105.2744
25	$2s2p3p\ ^4D_{1/2}$	78.7826		78.6446	93	$2p^23d\ ^4D_{1/2}$	86.9166		86.8019	161	$2s2p4f\ ^4D_{5/2}$	105.5769		105.2809
26	$2s2p3s\ ^2P_{3/2}$	79.0038		78.9506	94	$2p^23d\ ^4D_{5/2}$	86.9225		86.7780	162	$2s2p4f\ ^4G_{9/2}$	105.5812		105.2812
27	$2s2p3p\ ^4D_{3/2}$	79.0315		78.8880	95	$2p^23p\ ^2F_{5/2}$	87.1006		87.0175	163	$2s2p4p\ ^2D_{5/2}$	105.6051		105.4045
28	$2s2p3p\ ^2P_{3/2}$	79.3539	79.1710	79.2392	96	$2p^23d\ ^4D_{7/2}$	87.1807		87.0348	164	$2s2p4f\ ^2F_{5/2}$	105.6399		105.3291
29	$2s2p3p\ ^2P_{1/2}$	79.4356	78.2230	79.3193	97	$2p^23d\ ^4F_{9/2}$	87.2052		87.0496	165	$2s2p4f\ ^2G_{7/2}$	105.6411		105.3407
30	$2s2p3p\ ^4D_{5/2}$	79.4736		79.3473	98	$2p^23d\ ^4D_{3/2}$	87.2133		87.0765	166	$2s2p4p\ ^2S_{1/2}$	105.7184		105.5042
31	$2s2p3p\ ^4P_{1/2}$	79.6472		79.5906	99	$2p^23d\ ^2F_{5/2}$	87.2391		87.0956	167	$2s2p4d\ ^4F_{9/2}$	105.9131		105.6748
32	$2s2p3p\ ^2D_{3/2}$	79.8289	79.6400	79.7219	100	$2p^23p\ ^2F_{7/2}$	87.2453		87.1529	168	$2s2p4d\ ^4D_{7/2}$	105.9815	105.8710	105.7483
33	$2s2p3p\ ^4D_{7/2}$	80.1306		80.0262	101	$2p^23p\ ^2D_{3/2}$	87.4384		87.3288	169	$2s2p4d\ ^4D_{5/2}$	106.0086	105.8710	105.7785
34	$2s2p3p\ ^4P_{3/2}$	80.1878		80.1167	102	$2p^23s\ ^2S_{1/2}$	87.5428		87.5069	170	$2s2p4d\ ^4P_{3/2}$	106.0348		105.8077
35	$2s2p3p\ ^4P_{5/2}$	80.3448		80.2814	103	$2p^23p\ ^2D_{5/2}$	87.5843		87.4601	171	$2s2p4d\ ^4P_{1/2}$	106.0445		105.8212
36	$2s2p3p\ ^4S_{3/2}$	80.3676		80.2813	104	$2p^23d\ ^4P_{5/2}$	87.6294		87.4803	172	$2s2p4d\ ^2D_{5/2}$	106.1261	105.8070	105.8957
37	$2s2p3d\ ^4F_{3/2}$	80.4412		80.2645	105	$2p^23p\ ^2P_{1/2}$	87.7101		87.5900	173	$2s2p4d\ ^2P_{3/2}$	106.2272		105.9998
38	$2s2p3d\ ^4F_{5/2}$	80.6206		80.4371	106	$2p^23d\ ^4P_{3/2}$	87.7533		87.6056	174	$2s2p4d\ ^2F_{7/2}$	106.3120	106.1530	106.0809
39	$2s2p3p\ ^2D_{5/2}$	80.7846	80.6020	80.7160	107	$2p^23d\ ^2P_{1/2}$	87.7737		87.6772	175	$2s2p4f\ ^4F_{7/2}$	106.3383		106.0936
40	$2s2p3d\ ^4F_{7/2}$	80.9030	80.7750	80.7167	108	$2p^23d\ ^4P_{1/2}$	87.8428		87.7002	176	$2s2p4f\ ^4F_{9/2}$	106.3419		106.0959
41	$2s2p3d\ ^4P_{5/2}$	81.0112	80.8660	80.8151	109	$2p^23d\ ^2F_{7/2}$	87.8895		87.7481	177	$2s2p4f\ ^4F_{5/2}$	106.3576		106.1146
42	$2s2p3p\ ^2S_{1/2}$	81.0709		80.9981	110	$2p^23d\ ^2D_{5/2}$	88.2743		88.0947	178	$2s2p4d\ ^2P_{1/2}$	106.3625		106.1395
43	$2s2p3d\ ^4D_{3/2}$	81.0919	80.9390	80.9045	111	$2p^23d\ ^2D_{3/2}$	88.2917		88.1252	179	$2s2p4f\ ^2F_{7/2}$	106.3803		106.1337
44	$2s2p3s\ ^2P_{1/2}$	81.0922		81.0242	112	$2p^23p\ ^2P_{3/2}$	88.3428		88.2462	180	$2s2p4f\ ^4G_{11/2}$	106.3822		106.1341
45	$2s2p3s\ ^2P_{3/2}$	81.1217		81.0382	113	$2p^23d\ ^2G_{7/2}$	88.4228		88.3161	181	$2s2p4f\ ^4D_{3/2}$	106.3931		106.1525
46	$2s2p3d\ ^4D_{1/2}$	81.1303	80.9930	80.9331	114	$2p^23d\ ^2G_{9/2}$	88.5818		88.4689	182	$2s2p4f\ ^4D_{1/2}$	106.4193		106.1807
47	$2s2p3d\ ^2D_{3/2}$	81.4192		81.2526	115	$2p^23d\ ^2D_{3/2}$	88.8144		88.7219	183	$2s2p4f\ ^2G_{9/2}$	106.4221		106.1708

Notes. [a] MCDF calculation from the work of Jonauskas et al. (2006).

Table 5. Level energies (Ryd) of Kr^{31+} from different calculations, along with the compilation of NIST v4.

ID	Level	AS	NIST	Grasp[a]	ID	Level	AS	NIST	Grasp[a]	ID	Level	AS	NIST	Grasp[a]
1	$2s^22p\ ^2P_{1/2}$	0			69	$2p^23s\ ^2D_{3/2}$	173.0067		172.9762	137	$2s2p4p\ ^4D_{3/2}$	215.5095		
2	$2s^22p\ ^2P_{3/2}$	4.3704	4.4885	4.4815	70	$2s2p3d\ ^2F_{5/2}$	173.0532		172.9026	138	$2s2p4p\ ^4S_{3/2}$	215.6725		
3	$2s2p^2\ ^4P_{1/2}$	6.2363	6.3610	6.3565	71	$2s2p3d\ ^2D_{3/2}$	173.1556		172.9995	139	$2s2p4p\ ^4P_{1/2}$	215.9596		
4	$2s2p^2\ ^4P_{3/2}$	9.0192		9.2119	72	$2s2p3d\ ^2F_{7/2}$	173.1636		173.0084	140	$2s2p4d\ ^4F_{3/2}$	216.2201		
5	$2s2p^2\ ^4P_{5/2}$	10.3924	10.5186	10.5128	73	$2s2p3d\ ^2P_{1/2}$	173.5070		173.3435	141	$2s2p4p\ ^4D_{5/2}$	216.2695		
6	$2s2p^2\ ^2D_{3/2}$	12.9065	13.0261	13.0933	74	$2p^23p\ ^2S_{1/2}$	173.6190		173.5349	142	$2s2p4p\ ^2P_{1/2}$	216.2879		
7	$2s2p^2\ ^2P_{1/2}$	13.5508	13.6954	13.7905	75	$2s2p3d\ ^2D_{5/2}$	173.6270		173.4640	143	$2s2p4p\ ^2D_{3/2}$	216.3746		
8	$2s2p^2\ ^2D_{5/2}$	15.0204	15.2786	15.2515	76	$2p^23d\ ^4F_{3/2}$	173.7606		173.3439	144	$2s2p4d\ ^4P_{5/2}$	216.4855		
9	$2s2p^2\ ^2S_{1/2}$	18.2289	18.4936	18.5671	77	$2s2p3d\ ^2P_{3/2}$	173.8715		173.8828	145	$2s2p4f\ ^4G_{5/2}$	216.9139		
10	$2s2p^2\ ^2P_{3/2}$	18.3739	18.5837	18.6795	78	$2p^23p\ ^4P_{3/2}$	174.0082		173.6866	146	$2s2p4d\ ^4F_{5/2}$	216.9587		
11	$2p^3\ ^4S_{3/2}$	20.3589		20.6545	79	$2p^23d\ ^2F_{5/2}$	174.5572		174.1100	147	$2s2p4f\ ^4D_{7/2}$	217.0004		
12	$2p^3\ ^2D_{3/2}$	23.7137		24.0917	80	$2p^23p\ ^4P_{5/2}$	174.5847		174.4016	148	$2s2p4d\ ^4D_{3/2}$	217.1050		
13	$2p^3\ ^2D_{5/2}$	24.7156	24.9988	25.0107	81	$2p^23p\ ^4D_{5/2}$	175.0521		174.9006	149	$2s2p4d\ ^4D_{1/2}$	217.1475		
14	$2p^3\ ^2P_{1/2}$	26.4644		26.8755	82	$2p^23p\ ^4P_{1/2}$	175.2453		175.0895	150	$2s2p4d\ ^4F_{7/2}$	217.2121		
15	$2p^3\ ^2P_{3/2}$	29.8285	30.1338	30.2731	83	$2p^23p\ ^2D_{3/2}$	175.4975		175.3073	151	$2s2p4d\ ^2D_{3/2}$	217.3858		
16	$2s^23s\ ^2S_{1/2}$	154.6114		154.2276	84	$2p^23p\ ^4S_{3/2}$	175.8832		175.5995	152	$2s2p4d\ ^2F_{5/2}$	217.4336		
17	$2s^23p\ ^2P_{1/2}$	157.0706		156.6989	85	$2p^23p\ ^4D_{7/2}$	175.8952		175.6888	153	$2s2p4f\ ^4F_{3/2}$	217.6655		
18	$2s^23p\ ^2P_{3/2}$	158.2569		157.9555	86	$2p^23p\ ^2P_{3/2}$	176.3562		176.1610	154	$2s2p4f\ ^4G_{7/2}$	217.6753		
19	$2s2p3s\ ^4P_{1/2}$	159.4064		159.0764	87	$2p^23s\ ^2D_{5/2}$	176.6630		176.7414	155	$2s2p4f\ ^4D_{5/2}$	217.7037		
20	$2s2p3s\ ^4P_{3/2}$	160.1858		159.8467	88	$2p^23p\ ^2F_{5/2}$	176.7150		176.5184	156	$2s2p4f\ ^4F_{9/2}$	217.7466		
21	$2s^23d\ ^2D_{3/2}$	160.4971		160.1542	89	$2p^23d\ ^2P_{3/2}$	176.9355		176.7636	157	$2s2p4f\ ^2D_{5/2}$	217.7894		
22	$2s2p3s\ ^2P_{1/2}$	160.8956		160.6793	90	$2p^23d\ ^4F_{5/2}$	177.0666		176.8622	158	$2s2p4f\ ^2G_{7/2}$	217.8182		
23	$2s^23d\ ^2D_{5/2}$	160.9001		160.5432	91	$2p^23d\ ^4D_{1/2}$	177.0888		176.9279	159	$2s2p4s\ ^4P_{5/2}$	218.2805		
24	$2s2p3p\ ^4D_{1/2}$	161.5522		161.2021	92	$2p^23s\ ^2P_{3/2}$	177.0925		177.2024	160	$2s2p4s\ ^2P_{3/2}$	218.5739		
25	$2s2p3p\ ^4D_{3/2}$	162.2666		161.8959	93	$2p^23d\ ^4F_{7/2}$	177.2838		177.0555	161	$2s2p4p\ ^4P_{3/2}$	219.3617		
26	$2s2p3p\ ^4S_{3/2}$	163.1852		162.9443	94	$2p^23p\ ^2P_{1/2}$	177.3783		177.2319	162	$2s2p4p\ ^4P_{5/2}$	219.4165		
27	$2s2p3p\ ^4P_{1/2}$	163.2112		163.0068	95	$2p^23d\ ^4D_{7/2}$	177.7014		177.4653	163	$2s2p4p\ ^4D_{7/2}$	219.6924		
28	$2s2p3s\ ^4P_{5/2}$	163.6544		163.4560	96	$2p^23d\ ^4P_{5/2}$	177.8569		177.6161	164	$2s2p4p\ ^2P_{3/2}$	219.8072		
29	$2s2p3p\ ^2P_{1/2}$	163.7453		163.5031	97	$2p^23d\ ^4D_{3/2}$	177.8905		177.6662	165	$2s2p4p\ ^2D_{5/2}$	220.0000		
30	$2s2p3p\ ^4D_{5/2}$	163.8373		163.5706	98	$2p^23d\ ^4F_{9/2}$	178.1044		177.8244	166	$2s2p4p\ ^2S_{1/2}$	220.1217		
31	$2s2p3p\ ^2D_{3/2}$	164.1521		163.9029	99	$2p^23d\ ^4D_{5/2}$	178.5144		178.2427	167	$2s2p4d\ ^4F_{9/2}$	220.5868		
32	$2s2p3s\ ^2P_{3/2}$	164.5161		164.4218	100	$2p^23d\ ^4P_{3/2}$	178.6582		178.3838	168	$2s2p4d\ ^4D_{5/2}$	220.6171		
33	$2s2p3d\ ^4F_{3/2}$	164.8609		164.4521	101	$2p^23d\ ^4P_{1/2}$	178.7642		178.5213	169	$2s2p4d\ ^4D_{7/2}$	220.6221		
34	$2s2p3d\ ^4F_{5/2}$	165.4206		164.9840	102	$2p^23d\ ^2G_{7/2}$	179.1552		178.8820	170	$2s2p4d\ ^4P_{3/2}$	220.6604		
35	$2s2p3d\ ^4P_{5/2}$	165.9686		165.5013	103	$2p^23d\ ^2P_{1/2}$	179.1603		178.9874	171	$2s2p4d\ ^4P_{1/2}$	220.6734		
36	$2s2p3d\ ^4D_{3/2}$	166.2133		165.7409	104	$2p^23d\ ^2D_{5/2}$	179.1977		178.9137	172	$2s2p4d\ ^2D_{5/2}$	220.8715		
37	$2s2p3d\ ^4D_{1/2}$	166.2538		165.7826	105	$2p^23p\ ^2D_{3/2}$	179.3160		179.3183	173	$2s2p4d\ ^2P_{3/2}$	220.9922		
38	$2s2p3d\ ^4F_{7/2}$	166.2880		165.8234	106	$2p^23d\ ^2D_{3/2}$	179.3255		179.0596	174	$2s2p4d\ ^2F_{7/2}$	221.0962		
39	$2s2p3p\ ^4P_{3/2}$	166.3614		166.2384	107	$2p^23s\ ^2S_{1/2}$	179.5545		179.6339	175	$2s2p4d\ ^2P_{1/2}$	221.2045		
40	$2s2p3p\ ^4P_{5/2}$	166.5788		166.4449	108	$2p^23p\ ^2D_{5/2}$	179.5798		179.5502	176	$2s2p4f\ ^4F_{7/2}$	221.2142		
41	$2s2p3d\ ^2D_{3/2}$	166.9380		166.5049	109	$2p^23p\ ^2D_{5/2}$	179.8585		179.9361	177	$2s2p4f\ ^4F_{5/2}$	221.2379		
42	$2s2p3p\ ^4D_{7/2}$	167.1090		166.9917	110	$2p^23p\ ^2F_{7/2}$	179.9614		180.0311	178	$2s2p4f\ ^4G_{9/2}$	221.2520		
43	$2s2p3d\ ^2F_{5/2}$	167.1417		166.6575	111	$2p^23p\ ^2P_{1/2}$	180.0236		180.0891	179	$2s2p4f\ ^4D_{3/2}$	221.2916		
44	$2s2p3s\ ^2P_{1/2}$	167.2047		167.1139	112	$2p^23p\ ^2P_{3/2}$	181.6660		181.7500	180	$2s2p4f\ ^2F_{7/2}$	221.3237		
45	$2s2p3p\ ^2P_{3/2}$	167.3422		167.2395	113	$2p^23p\ ^2P_{1/2}$	181.9045		182.0360	181	$2s2p4f\ ^4G_{11/2}$	221.3333		
46	$2s2p3s\ ^2P_{3/2}$	167.3538		167.2602	114	$2p^23d\ ^2F_{7/2}$	182.0481		182.0734	182	$2s2p4f\ ^4D_{1/2}$	221.3349		
47	$2s2p3p\ ^2D_{5/2}$	167.9892		167.9185	115	$2p^23d\ ^2G_{9/2}$	182.2235		182.2292	183	$2s2p4f\ ^2G_{9/2}$	221.3642		

Notes. [(a)] GRASP calculation with QED-correction from the work of Aggarwal et al. (2008).

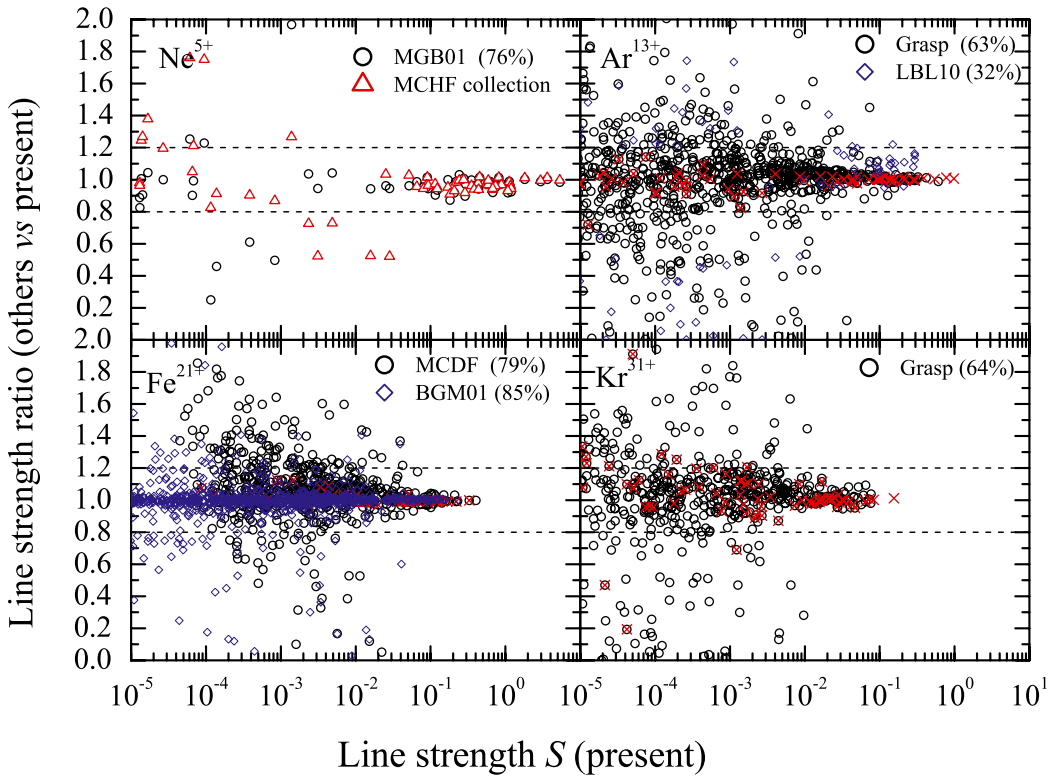

Fig. 1. Comparison of line strengths (S) of electric-dipole transitions for ions spanning the sequence. For Ne^{5+}, MGB01 corresponds to the MCHF calculation of Mitnik et al. (2001) for transitions among the lowest 20 levels, while "up-triangle" symbols correspond to the data from the MCHF/MCDF collection[6]. For Ar^{13+}, comparisons are made with the GRASP calculation by Aggarwal et al. (2005) and with the AUTOSTRUCTURE calculation by Ludlow et al. (2010, hereafter LBL10) for all transitions amongst levels of the $n = 2$ configurations. The "×" symbols denote transitions among the lowest 20 levels. For Fe^{21+}, a comparison is made with the MCDF calculation (Jonauskas et al. 2006) and that of Badnell et al. (2001, hereafter BGM01) for all transitions amongst levels of the $n = 2$ configurations. The "×" symbols are the same as for Ar^{13+}. For Kr^{31+}, we compare with the GRASP calculation by Aggarwal et al. (2008). The horizontal dashed lines correspond to an agreement within 20%.

The present AS calculation agrees well with the GRASP calculation, to within 1%, and even better than 0.5% for most levels, see Table 3. In the work of Ludlow et al. (2010)[4], the orbital scaling parameters were adjusted by hand to bring the calculated $n = 2$ level energies into close agreement with the NIST v4 experimental values. But our ab initio results agree much better with the NIST values for the $n = 3$ and 4 levels. For compactness, we do not present their results in Table 3. We do note that the Ludlow et al. (2010) *R*-matrix calculations covered the whole argon isonuclear sequence and so they were constrained to use a simplified structure. With an isoelectronic sequence, once we have determined the best approach to the structure for one ion, the same one works with little change for every other one of the sequence (excluding near neutral).

For Fe^{21+}, Jonauskas et al. (2006) performed an unprecedented large-scale calculation using the multi-configuration Dirac-Fock (MCDF) approach with the promotion of one, two, and three electrons from $n = 2$ to all possible combinations of one, two, or three electrons in the shells up to $n = 3$. The present AS level energies agree within 0.5% for all levels of $n = 3$ and 4 configurations. For low-lying levels of $n = 2$ complex, the difference is still within 2%, see Table 4. Badnell et al. (2001) performed a similar calculation to the present one, but without inclusion of $2s3l3l'$ and $2p3s3l$ configurations, again using the AUTOSTRUCTURE code[5]. Their resulting level energies show an excellent agreement with the present ones. Due to the similarity of the two approaches, their results are not listed in Table 4.

For the highly charged case of Kr^{31+}, the most recent theoretical work is the fully relativistic GRASP calculation performed by Aggarwal et al. (2008). Table 5 shows that the present AS calculation agrees to better than 1% with the GRASP calculation.

2.2. Structure: line strength S

Another test of our structure calculation is to compare line strengths (S_{ij} for a given $i \leftarrow j$ transition). In terms of the transition energy E_{ji} (Ryd) for the $j \rightarrow i$ transition, the absorption oscillator strength, f_{ij}, can be written as

$$f_{ij} = \frac{E_{ji}}{3g_i} S, \tag{1}$$

and the transition probability or Einstein's A-coefficient, A_{ji}, as

$$A_{ji}(\text{au}) = \tfrac{1}{2}\alpha^3 \frac{g_i}{g_j} E_{ji}^2 f_{ij}, \tag{2}$$

where α is the fine structure constant, and g_i, g_j are the statistical weight factors of the initial and final states, respectively.

Figure 1 illustrates a graphical comparison of line strengths with previous calculations for electric-dipole transitions for the four representative ions. For the lower charged Ne^{5+} ion, 76%

[4] Ballance provided us with their results for Ar^{13+} in the adf04 file format (priv. comm.).

[5] Their resulting data are available from the Open-ADAS database in the adf04 file format.

of all possible transitions among the lowest 20 levels agree with the MCHF calculation (Mitnik et al. 2001) to within 20%. Mitnik et al. (2001) demonstrated that the average difference is 24% between their results and the data from MCHF/MCDF collection database[6]. We illustrate this comparison again by "up-triangle" symbols in the top-left panel in Fig. 1, which reveals a comparable level of agreement with that in Table 2 of Mitnik et al. (2001).

For Ar^{13+}, the 460-level GRASP calculation performed by Aggarwal et al. (2005) is the largest-scale work for this ion to our best knowledge. We provide a comparison with their results, again in Fig. 1. There are 63% of all electric-dipole transitions to levels of n =2 configurations which agree to within 20% between the two different calculations. For transitions among the lowest 20 levels, an even better (84%) agreement is found. The data from Ludlow et al. (2010) show a worse agreement with ours. There are only 32% of all available transitions to $n = 2$ levels to agree within 20%. Even for transitions within $n = 2$ levels, the percentage is 53%. Their lack of an optimized structure is likely the cause. Additionally, their radiative decay rate (A_{ij}) values in adf04 file were scaled according the theoretical and NIST level energies. That might also contribute to some of the low percentage in the differences of dipole line strengths.

For Fe^{21+}, the work of Jonauskas et al. (2006) is likley the largest-scale calculation. The present AS calculation agrees with their results to within 20% for 79% of all electric-dipole transitions to levels of $n = 2$ complex. In comparison with the results of Badnell et al. (2001), 85% of all electric-dipole transitions to $n = 2$ levels agree within 20%. This difference is attributed to the CI effect from the $2s3l3l'$ and $2p3s3l$ configurations included in our AS calculation.

For the highly charged case of Kr^{31+}, a comparison is made with the GRASP calculation of Aggarwal et al. (2008). There are 64% of all transitions to levels of $n = 2$ that agree to within 20%. For transitions within $n = 2$ levels, the percentage is 92%.

The scatter plots show that the deviations between the present AS calculation and various previous results are much stronger and more widespread for the weaker transitions than the strong ones, as expected.

Overall, the atomic structure of the ions spanning the sequence is reliable, and the uncertainty in collision strengths (Ωs) due to inaccuracies in the target structure is correspondingly small.

3. Scattering

The present parallel ICFT R-matrix calculations employed 40 continuum basis orbitals per angular momentum to represent the $(N + 1)$th-electron over the sequence. All partial waves from $J = 0$ to 41 were included explicitly and the contribution from higher J-values was included using a "top-up" procedure (Burgess 1974; Badnell & Griffin 2001). The contribution from partial waves up to $J = 12$ included electron exchange while those from $J = 13$ to 41 were non-exchange, calculated using the exchange R-matrix code in its non-exchange mode. For the exchange calculation, a fine energy mesh was used to resolve the majority of narrow resonances below the highest excitation threshold, which has been tested to be sufficient for the convergence of the effective collision strength, see Fig. 2. From just above the highest threshold excitation to a maximum energy of ten times the ionization potential for each ion, a coarse energy mesh ($1.0 \times 10^{-3}\ z^2$ Ryd, where $z = Z-5$ is the residual charge of ion) was employed. For the non-exchange calculation, a step of $1.0 \times 10^{-3}\ z^2$ Ryd was used over the entire energy range. Additionally, experimentally determined energies or adjusted energies were employed in the MQDT expressions used by the ICFT method to further improve the accuracy of the results, as was done for highly charged sulphur ions (Liang et al. 2011). The lowest-lying 8 LS terms (15 IC levels) of the $n = 2$ complex were corrected for almost all ions over the iso-electronic sequence, as explained in detail in the structure section.

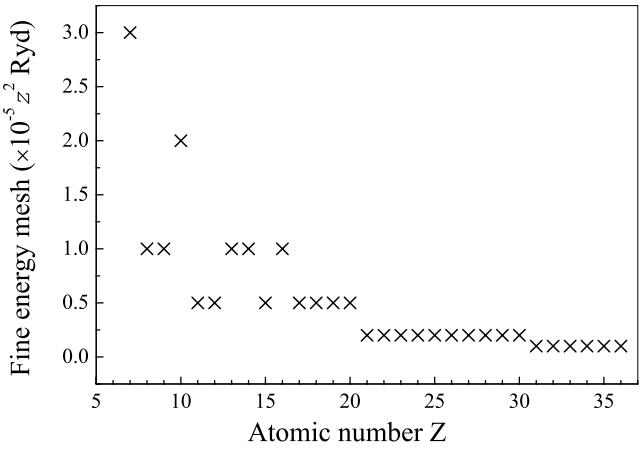

Fig. 2. Fine energy mesh employed in the outer region (exchange) R-matrix calculation for each ion.

As mentioned in the introduction, we wish to determine excitation data for the 204 CC levels of the $2s^x2p^y$ $(x + y = 3)$, $2s^2\{3,4\}l$, $2s2p\{3,4\}l$, and $2p^23l$ configurations. But for some ions, these do not correspond to the lowest energy 204 levels (92 LS terms). When this occurs, we include additional terms in the close-coupling expansion so that all $2p^23l$ levels are still in the close-coupling expansion and there are no "gaps" below them. For example, for N^{2+} and O^{3+}, the $2p^24s$ $^4P/^2P$, $2p^24p$ $^2S/^4P/^4D$ terms were included.

To take the contribution from higher electron energies to high temperature effective collision strengths into account, the infinite energy Born limits (non-dipole allowed) and line strengths (dipole allowed) from AUTOSTRUCTURE were used to obtain collision strengths (Ω) at higher energies according to the procedure defined by Burgess & Tully (1992). The effective collision strengths at 13 electron temperatures ranging from $2 \times 10^2\ (z + 1)^2$ K to $2 \times 10^6 (z + 1)^2$ K are produced as the end product with ADAS adf04 format (Summers 2004).

4. Results and discussions

4.1. Comparison with previous calculations

As in our other iso-electronic sequence work, we selected several transitions to test the original collision strength for four ions (Ne^{5+}, Ar^{13+}, Fe^{21+} and Kr^{31+}) spanning over the sequence. An extensive comparison for effective collision strength will be given by a scatter plot to test how far the reliability reaches.

– Ne^{5+} Mitnik et al. (2001) performed a 180-level ICFT R-matrix calculation for this ion with the same CC expansion as we did except for the 2s2p4f configuration. As mentioned above, the MCHF approach was used to describe the target structure and three pseudo-orbitals were included to partially correct spectroscopic orbitals in this previous calculation. Our 204-level collision strength shows an excellent

[6] http://nlte.nist.gov/MCHF/view.html

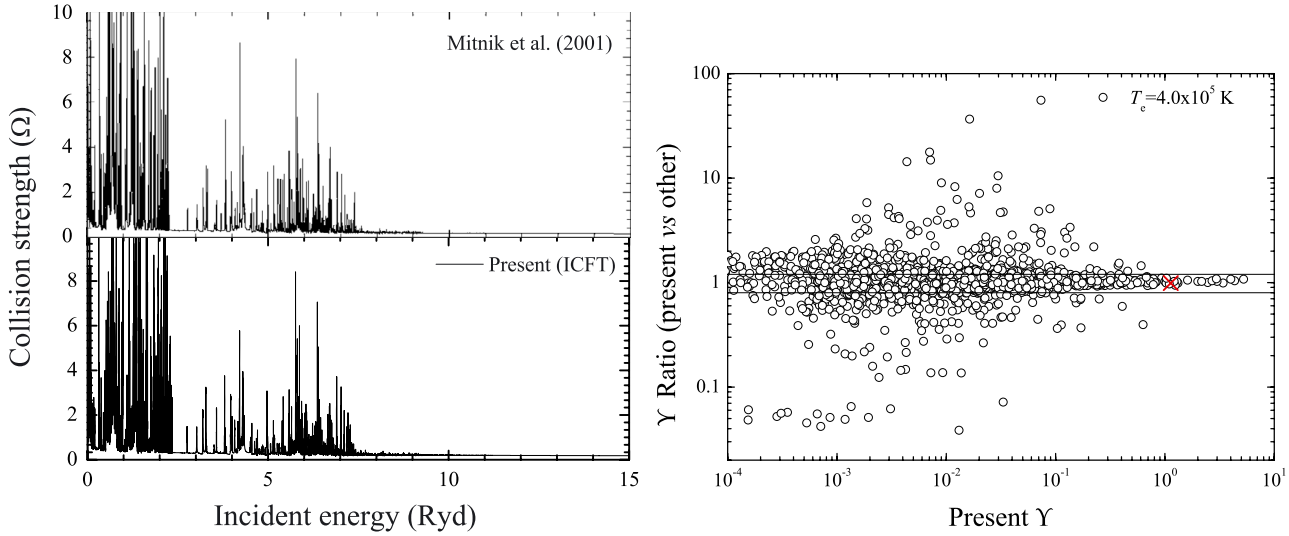

Fig. 3. (Effective) collision strengths for Ne^{5+}. *Left*: excitation from the $2s^2 2p\ ^2P_{1/2}$ ground level to the $2s^2 2p\ ^2P_{3/2}$ level (1–2). *Right*: excitations amongst all 15 levels of the $n = 2$ configurations at the temperature ($T_e = 4.0 \times 10^5$ K) of peak fractional abundance in ionization equilibrium. The (red) "×" marks the 1–2 excitation shown in the lefthand panel. Double-horizontal lines correspond to agreement within 20%. *Notes: the collision strength of Mitnik et al. (2001) is a scanned picture.*

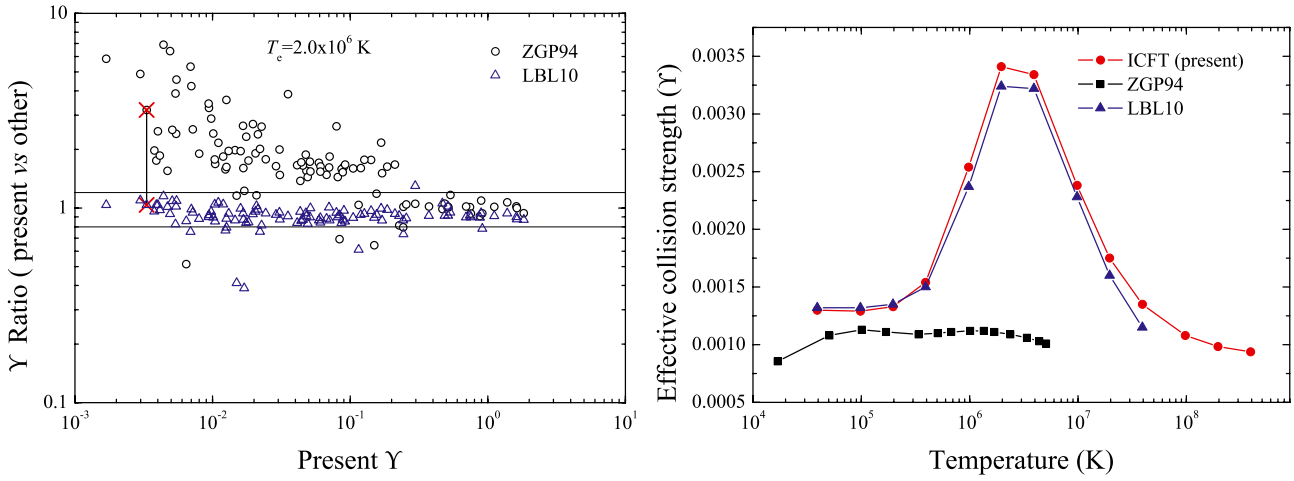

Fig. 4. Comparison of effective collision strengths for Ar^{13+}. *Left*: all excitations among the 15 levels of the $n = 2$ configurations at the temperature ($T_e = 4.0 \times 10^6$ K) of peak fractional abundance in ionization equilibrium. The "×" symbol corresponds to the $2s^2 2p\ ^2P_{3/2}$–$2p^3\ ^2P_{3/2}$ (1–15) excitation shown in the righthand panel, which is linked for the two different previous calculations. Double-horizontal lines correspond to agreement within 20%. *Right*: the effective collision strength of the 1–15 transition as a function of temperature (K). ZGP94 and LBL10 correspond to the Breit-Pauli *R*-matrix works of Zhang et al. (1994) and Ludlow et al. (2010), respectively.

agreement with this previous one, see left panel in Fig 3. An extensive comparison of effective collision strength is given in the right panel of Fig. 3 for all excitations from levels of $n = 2$ configurations at a temperature of peak fraction in ionization equilibrium. About 73% of the excitations agree within 20%.

– Ar^{13+} The small-scale ($n = 2$) *R*-matrix calculation performed by Zhang et al. (1994) is extensively adopted by various databases, e.g. Open-ADAS[7] and Chianti v7 (Landi et al. 2012). Comparison with these data for all excitations among the 15 lowest-lying levels reveals that the previous *R*-matrix data are systematically lower than ours, and the deviations are stronger for weaker excitations, see Fig. 4. However, the data from the work of Ludlow et al. (2010) agree well with ours even though only 36 IC levels of $(1s^2)2s^x 2p^y$ ($x + y = 3$), $2s^2\{3, 4, 5\}l$ configurations were included in their close-coupling expansion. Ninety percent of all transitions within $n = 2$ levels agree to within 20%. For the $2s^2 2p\ ^2P_{3/2}$–$2p^3\ ^2P_{3/2}$ (1–15) excitation, there is an obvious bump in the present ICFT *R*-matrix calculation at temperatures of 10^6–10^7 K, with the difference being up to ∼3.5 when compared with Zhang et al.'s data. This is an obvious enhancement due to resonances attached to $n = 3$ that were not included in the previous small-scale calculation. The good agreement with Ludlow et al.'s data also supports this.

– Fe^{21+} After carrying out a level mapping procedure according to $LS\,J^\pi$ and configurations, an extensive comparison was made with a previous (204-level) ICFT *R*-matrix calculation (Badnell et al. 2001) at three temperatures of 10^5, 10^6, and

[7] http://open.adas.ac.uk/

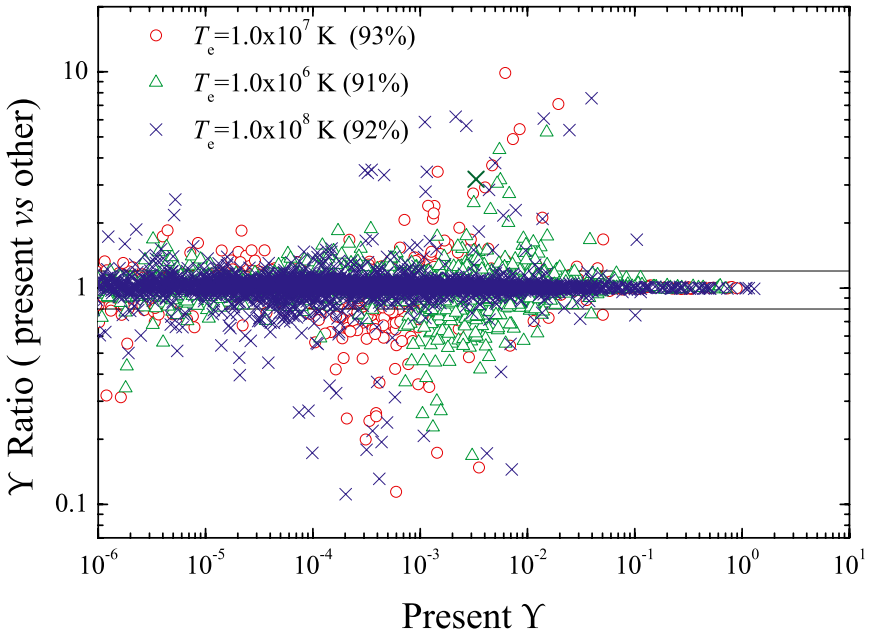

Fig. 5. Comparison of effective collision strength with the results of Badnell et al. (2001) for Fe^{21+} for all excitations from the lowest 15 levels at temperatures of $T_e = 1.0 \times 10^6, 10^7$ and 10^8 K. Double-horizontal lines correspond to agreement within 20%.

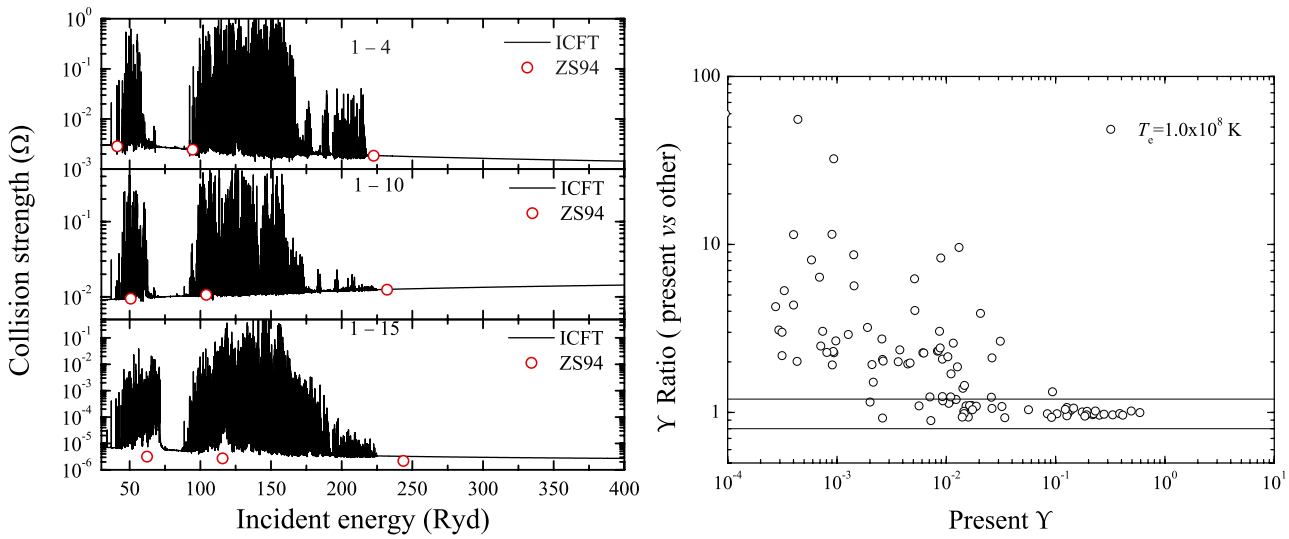

Fig. 6. (Effective) collision strengths for Kr^{21+}. *Left*: present collision strengths for $2s^22p\ ^2P_{1/2}$–$2s2p^2\ ^4P_{3/2}$ (1–4), $2s^22p\ ^2P_{1/2}$–$2s2p^2\ ^2P_{3/2}$ (1–10), and $2s^22p\ ^2P_{1/2}$–$2p^3\ ^2P_{3/2}$ (1–15) transitions along with the distorted-wave calculation by Zhang & Sampson (1994a, ZS94). *Right*: ratio of effective collision strength between the present ICFT *R*-matrix calculation and DW results available from the Open-ADAS database[7] at a temperature of 1.0×10^8 K. Double-horizontal lines correspond to agreement within 20%.

10^7 K. Almost all excitations (93%) agree to within 20% for the two different calculations with a different target structure, see Fig. 5. The differences between them and the widespread agreement do not change much with increasing temperature. This results from the consistent resonance structure in the two calculations. Badnell et al. (2001) made a detailed assessment for their calculation with previous available data, therefore we will not repeat the comparison here.

– Kr^{31+} To our best knowledge, there are no *R*-matrix excitation data available for this ion. Therefore, we compared the background of the present ICFT *R*-matrix calculation with that from a distorted-wave calculation performed by Zhang & Sampson (1994a,b) for excitations from the ground level $2s^22p\ ^2P_{1/2}$. Figure 6 illustrates some excitations from this comparison. The background of the collision strengths agrees well with the DW calculation. As expected, the present effective collision strengths Υ are systematically higher than those from the distorted-wave approach due to the inclusion of resonances.

From the above comparison for the four specified ions (Ne^{5+}, Ar^{13+}, Fe^{21+} and Kr^{31+}) spanning the iso-electronic sequence, we believe the present ICFT *R*-matrix results (Ω and Υ) to be reliable. For ions near neutral (below O^{3+}), *R*-matrix with pseudostates calculations are needed to consider ionization loss in the excitation, but ours are the best data available to date.

4.2. Trends of iso-electronic sequence

As in our previous sequence works (Witthoeft et al. 2007; Liang et al. 2009c, 2010, 2011), we take configuration, total angular

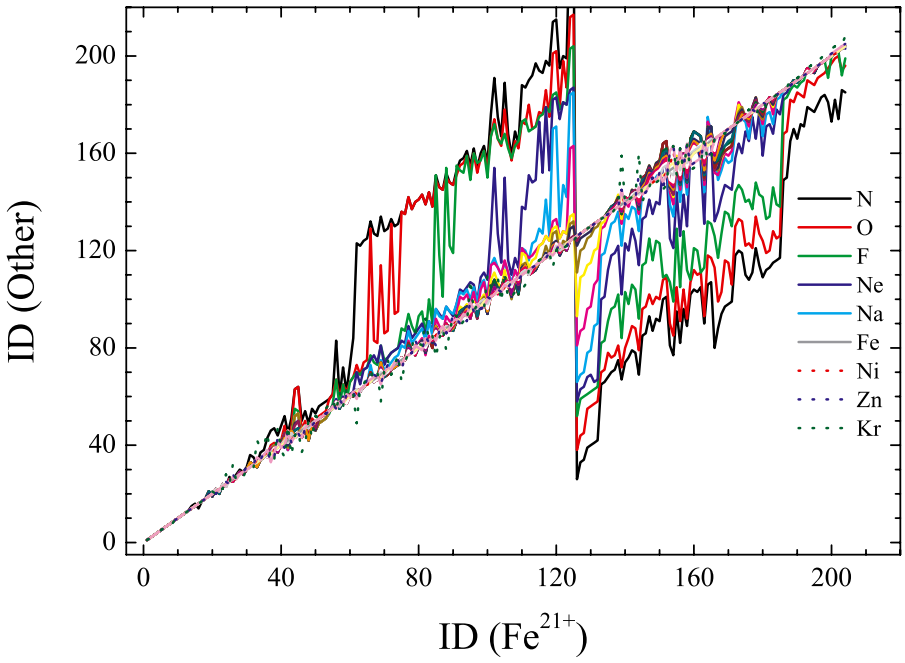

Fig. 7. Level ordering with the original level index (ID) relative to the ordering of Fe^{21+} by mapping according to the "good" quantum numbers – configuration, total angular momentum J, and energy ordering for ions spanning the entire sequence. The spikes and dips are due to the shift of a given level, for example, $2p^2 3s\ ^4P$ (62–65) levels in Fe^{21+} move to levels above 120 in N^{2+}.

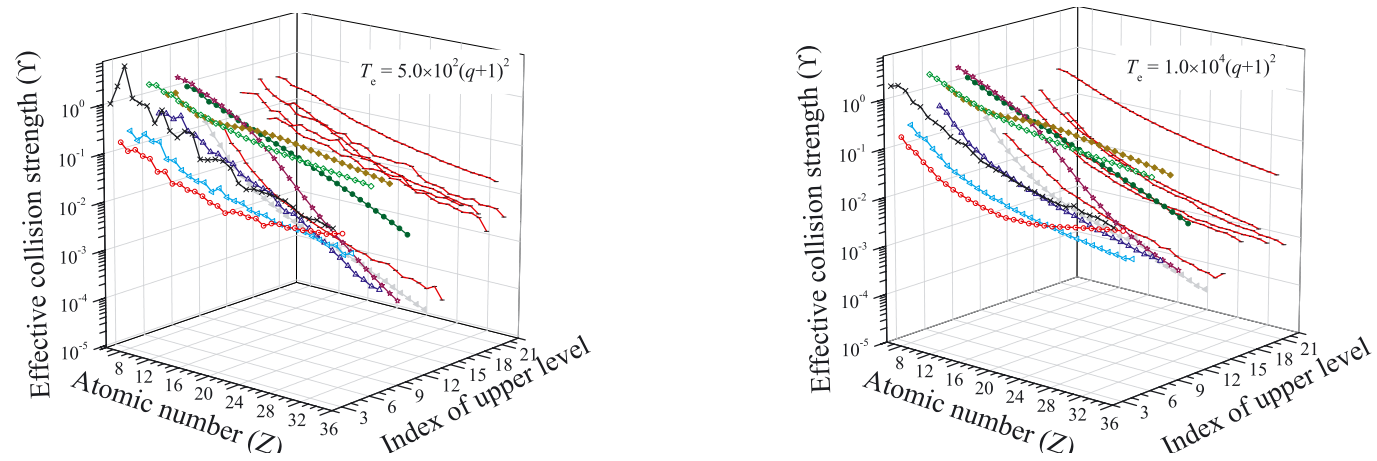

Fig. 8. Effective collision strength (ϒ) for excitations from the ground level to all 22 lowest-lying excited levels at temperatures of $T_e = 5\times10^2(q+1)^2$ and $1\times10^4(q+1)^2$ K (here $q = Z-5$) along the iso-electronic sequence. *Notes: the index number refers to the ID number in the reference ion – Fe.*

momentum J, and energy ordering as a good quantum number for level matching in the comparison between different calculations and the investigation of ϒ along the iso-electronic sequence, see Fig. 7. This satisfactorily eliminates uncertainty originating from the non-continuity of level-ordering along the sequence. We used Fe as the arbitrary reference ion for the level-ordering.

In Fig. 8, we show the effective collision strength ϒ at temperatures of $T_e/(q+1)^2 = 5\times10^2$ and 10^4 K along the iso-electronic sequence for excitations from the ground level to the lowest-lying (in Fe^{21+}) 22 excited levels. At the low temperature of $5\times10^2(q+1)^2$ K, spikes and/or dips are observed at low charges for some transitions, e.g. $2s^2 2p\ ^2P_{1/2} \rightarrow 2s^2 2p\ ^2P_{3/2}$ (1−2). With increasing threshold energy, that is to higher excited levels, this irregularity becomes weaker and eventually disappears. At the high temperature of $1\times10^4(z+1)^2$ K, the spikes and/or dips disappear, as expected, because the resonance contribution becomes weaker and eventually negligible.

5. Summary

We have performed 204-level ICFT *R*-matrix calculations for the electron-impact excitation of all ions of the boron-like iso-electronic sequence from C^+ to Kr^{31+}.

Good agreement with the available experimentally derived data and the results of others for level energies and line strengths S for several specific ions (Ne^{5+}, Ar^{13+}, Fe^{21+}, and Kr^{31+}) spanning the iso-electronic sequence, supports the reliability of our *R*-matrix excitation data. This was confirmed specifically by detailed comparisons of Ω and/or ϒ with previous *R*-matrix calculations, where available, for the four specific reference ions.

Our *R*-matrix excitation data are expected to be an important improvement on the current data (from relativistic distorted-wave approach), which are extensively used by the spectroscopic diagnostic modelling communities in astrophysics and magnetic fusion.

By excluding the level-crossing effects on the Υ, we examined the iso-electronic trends of the effective collision strengths. As expected, a complicated pattern of spikes and dips of Υ at low temperatures was noted again along the sequence as shown in our other series works.

The data are made available in the ADAS *adf04* format (Summers 2004) at the archives of the APAP[2], OPEN-ADAS[7] and will be included in the CHIANTI[8] database. At the APAP-network website[2], the original collision strength also can be made available.

In conclusion, we have generated an extensive set of reliable excitation data with the ICFT *R*-matrix method for spectroscopy/diagnostic research within the astrophysical and fusion communities. This will replace the data from DW and small-scale *R*-matrix calculations presently used by these communities, and it is expected to identify new lines and may overcome some shortcomings in present astrophysical modelling.

Acknowledgements. We thank Connor Ballance at Auburn University for helpful comments. The work of the UK APAP Network is funded by the UK STFC under grant No. ST/J000892/1 with the University of Strathclyde. GYL acknowledges the support from the One-Hundred-Talents programme of the Chinese Academy of Sciences (CAS). G.Z. acknowledges the support from National Natural Science Foundation of China under grant No. 10821061.

References

Acton, L. W., Bruner, M. E., Brown, W. A., et al. 1985, ApJ, 291, 865
Aggarwal, K. M., Keenan, F. P., & Nakazaki, S. 2005, A&A, 436, 1141
Aggarwal, K. M., Keenan, F. P., & Lawson, K. D. 2008, At. Data Nucl. Data Tables, 94, 323
Badnell, N. R. 1986, J. Phys. B: At. Mol. Opt. Phys., 19, 3827
Badnell, N. R., & Griffin, D. C. 2001, J. Phys. B: At. Mol. Opt. Phys., 34, 681
Badnell, N. R., Griffin, D. C., & Mitnik, D. M. 2001, J. Phys. B: At. Mol. Opt. Phys., 34, 5071
Brown, C. M., Feldman, U., Seely, J. F., et al. 2008, ApJS, 176, 511
Burgess, A. 1974, J. Phys. B: At. Mol. Opt. Phys., 7, L364
Burgess, A., & Tully, J. A. 1992, A&A, 254, 436
Del Zanna, G. 2012, A&A, 537, A38
Del Zanna, G., Storey, P. J., Badnell, N. R., & Mason, H. E. 2012, A&A, 543, A139
Flower, D. R., & Nussbaumer, H. 1975, A&A, 45, 349
Foster, A. R., Ji, L., Smith, R. K., & Brickhouse, N. S. 2012, ApJ, 756, 128
Griffin, D. C., Badnell, N. R., & Pindzola, M. S. 1998, J. Phys. B: At. Mol. Opt. Phys., 31, 3713
Huber, M. C. E., Dupree, A. K., Goldberg, L., et al. 1973, ApJ, 183, 291
Jonauskas, V., Bogdanovich, P., Keenan, F. P., et al. 2006, A&A, 455, 1157
Keenan, F. P., O'Shea, E., & Thomas, R. J. 2000, MNRAS, 315, 450
Keenan, F. P., Katsiyannis, A. C., Ryans, R. S. I., et al. 2002, ApJ, 566, 521
Landi, E., & Young, P. R. 2009, ApJ, 706, 1
Landi, E., Del Zanna, G., Young, P. R., et al. 2012, ApJ, 744, 99
Liang, G. Y., & Badnell, N. R. 2010, A&A, 518, A64
Liang, G. Y., & Badnell, N. R. 2011, A&A, 528, A69
Liang, G. Y., & Zhao, G. 2008, AJ, 135, 2291
Liang, G. Y., & Zhao, G. 2010, MNRAS, 405, 1987
Liang, G. Y., Whiteford, A. D., & Badnell, N. R. 2008, J. Phys. B: At. Mol. Opt. Phys., 41, 235203
Liang, G. Y., Whiteford, A. D., & Badnell, N. R. 2009a, A&A, 499, 943
Liang, G. Y., Whiteford, A. D., & Badnell, N. R. 2009b, A&A, 500, 1263
Liang, G. Y., Whiteford, A. D., & Badnell, N. R. 2009c, J. Phys. B: At. Mol. Opt. Phys., 42, 225002
Liang, G. Y., Badnell, N. R., Zhao, G. 2011, A&A, 533, A87
Ludlow, J. A., Ballance, C. P., Loch, S. D., & Pindzola, M. S. 2010, J. Phys. B: At. Mol. Opt. Phys., 43, 074029
Malinovsky, M., & Heroux, L. 1973, ApJ, 181, 1009
Mitnik, D. M., Griffin, D. C., & Badnell, N. R. 2001, J. Phys. B: At. Mol. Opt. Phys., 34, 4455
Peng, J. F., & Pradhan, A. K. 1995, A&AS, 112, 151
Summers, H. P. 2004, The ADAS User manual version 2.6, http://www.adas.ac.uk/
Witthoeft, M. C., Whiteford, A. D., & Badnell, N. R. 2007, J. Phys. B: At. Mol. Opt. Phys., 40, 2969
Zhang, H. L., & Sampson, D. H. 1994a, At. Data Nucl. Data Tables, 56, 41
Zhang, H. L., & Sampson, D. H. 1994b, At. Data Nucl. Data Tables, 58, 255
Zhang, H. L., Graziani, M., & Pradhan, A. K. 1994, A&A, 283, 319

[8] http://www.chianti.rl.ac.uk/